

Computational Simulation of Extravehicular Activity Dynamics During a Satellite Capture Attempt

Grant Schaffner* and Dava J. Newman†
Massachusetts Institute of Technology,
Cambridge, Massachusetts 02139

and

Stephen K. Robinson‡
NASA Johnson Space Center, Houston, Texas 77058

Introduction

A MORE quantitative approach to the analysis of astronaut extravehicular activity (EVA) tasks is needed because of their increasing complexity, particularly in preparation for the on-orbit assembly of the International Space Station. Existing useful EVA computer analyses produce either high-resolution three-dimensional computer images based on anthropometric representations^{1,2} or empirically derived predictions of astronaut strength based on lean body mass and the position and velocity of body joints³ but do not provide multibody dynamic analysis of EVA tasks.

Our physics-based methodology helps fill the current gap in quantitative analysis of astronaut EVA by providing a multisegment human model and solving the equations of motion in a high-fidelity simulation of the system dynamics. The simulation work described here improves on the realism of previous efforts⁴ by including three-dimensional astronaut motion, incorporating joint stops to account for the physiological limits of range of motion, and making use of constraint forces to model interaction with objects.

To demonstrate the utility of this approach, the simulation is modeled on an actual EVA task, namely, the attempted capture of a spinning Intelsat VI satellite during STS-49 in May 1992. Repeated capture attempts by an EVA crewmember were unsuccessful because the capture bar could not be held in contact with the satellite long enough for the capture latches to fire and successfully retrieve the satellite.

Methods

The dynamic system model includes three elements: the satellite, capture bar, and astronaut (Fig. 1). A single rigid body represents the Intelsat VI satellite with six degrees of freedom (dof) initially rotating around the X (roll) axis at a rate of 1 rpm. The structural interface ring (where contact with the capture bar occurs) has a diameter of 2.35 m and is located 1.34 m from the satellite's center of mass (in the X direction). The capture bar is also represented by a single rigid body with six dof; assistive v-guides are situated 2.35 m apart and the astronaut manipulation wheel has a diameter of 0.29 m. The center of mass of the capture bar is 0.81 m to the right of the center of the manipulation wheel and 0.31 m behind the front surface. The astronaut is modeled as a 12-segment system: right and left lower leg, upper leg, upper arm, lower arm, and hand; pelvis; and combined torso/head/primary life support system (PLSS). Three-dof ball joints define the ankle, hip, sacroiliac, shoulder, and wrist joints; single-dof hinge joints define the knees and elbows. The astronaut model has 31 dof, allowing full three-dimensional movement capability. The mass properties and joint parameters for the system are presented in Table 1.

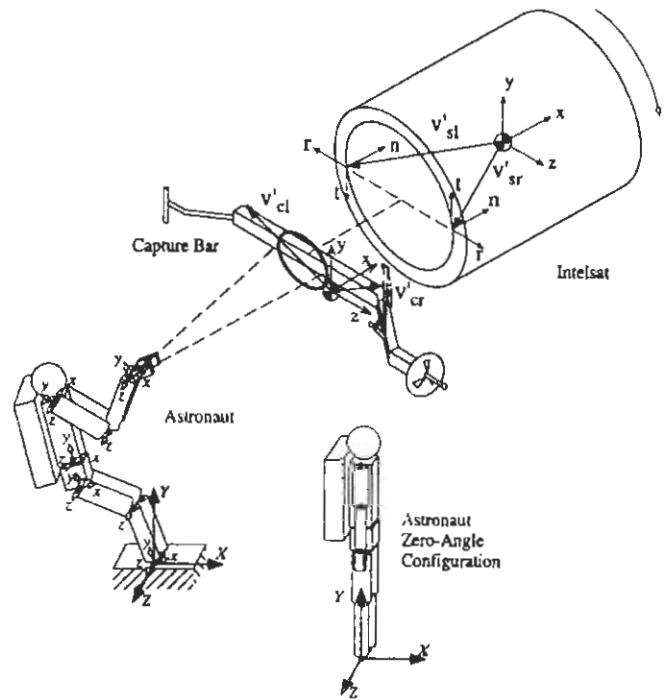


Fig. 1 Dynamic system: multibody astronaut model, Intelsat VI satellite, and capture bar.

The complete dynamic system (satellite, capture bar, and astronaut) has 43 dof. Because it is intractable to derive the equations of motion for such a complex multibody system by hand, a commercial program (SD/FAST, Symbolic Dynamics, Inc., Mountain View, California) was used to produce computer code representing the equations of motion. The simulation itself is run by computer code developed by the authors and is divided into two phases: an inverse-kinematics phase that uses the modeling and control schemes described later to compute the motion of the system, and an inverse-dynamics phase that uses these recorded motions to compute the astronaut's body joint torques.

During the inverse-kinematics phase, constraint forces are used to model the interaction between the capture bar and the satellite. As the capture bar comes into contact with the satellite, the amount of deviation δ_r and δ_l between the optimal contact points on the right- and left-hand sides is found from

$$\delta_r = v_{cr} - v_{sr}, \quad \delta_l = v_{cl} - v_{sl} \quad (1)$$

where v_{cr} and v_{cl} are the global (inertial) reference frame transforms of vectors V'_{cr} and V'_{cl} (Fig. 1), which locate the contact points in the capture bar's body reference frame, and v_{sr} and v_{sl} are the global transforms of V'_{sr} and V'_{sl} , which locate the contact points in the satellite's body reference frame.

The following discussion applies equally to right- and left-hand sides. During contact, constraint forces are modeled as springs and dampers acting in the normal and radial directions (defined by unit vectors n and r in Fig. 1):

$$F_n = K_n \delta_n + B_n \dot{\delta}_n, \quad F_r = K_r \delta_r + B_r \dot{\delta}_r \quad (2)$$

where F_n and F_r are the constraint forces, δ_n and δ_r the components of the deviation vector, K_n and K_r the stiffness coefficients, and B_n and B_r the damping coefficients, in the normal and radial directions, respectively. The values chosen for the stiffness and damping coefficients were obtained partly from material properties and partly from trial and error. The final values used for K_n and K_r were 1000 and 500 N/m, respectively, and 50 Ns/m was used for both B_n and B_r . The force in the tangential direction (unit vector t in Fig. 1) arises from friction between the rotating satellite ring and the capture bar:

$$F_t = \mu F_n \quad (3)$$

where μ , the coefficient of friction, was set at 0.25.

Received 31 March 1998; revision received 1 November 1998; accepted for publication 10 June 1999. Copyright © 1999 by the American Institute of Aeronautics and Astronautics, Inc. All rights reserved.

*Research Assistant, Department of Aeronautics and Astronautics, Room 37-219.

†Associate Professor of Aeronautics and Astronautics, Room 33-407, Member AIAA.

‡Astronaut.

Table 1 Mass, inertia, angle, stiffness, and damping properties for all objects in the dynamic system^a

Segment/ Object	Mass, kg	Moments of inertia, kgm ² (body-fixed coordinates)			Joint	Initial angle (right/left), deg			Stiffness, <i>k</i> Nm/deg	Damping, <i>b</i> Nms/deg
		<i>I_{xx}</i>	<i>I_{yy}</i>	<i>I_{zz}</i>		Roll	Yaw	Pitch		
Intelsat	4065.00	6781.000	6114.000	6140.000	6 dof	—	—	—	—	—
Capture bar	73.21	71.763	87.579	15.869	6 dof	—	—	—	—	—
Hand	0.53	0.001	0.001	0.001	Wrist	0/0	0/0	-55/-55	0.70	0.35
Forearm	1.45	0.009	0.001	0.010	Elbow	—	—	90/90	0.70	0.35
Upper arm	2.05	0.014	0.003	0.015	Shoulder	-90/90	0/0	55/55	0.70	0.35
Head	5.50	0.021	0.015	0.024	—	—	—	—	—	—
Trunk	28.61	0.531	0.332	0.392	Sacroiliac	0	0	0	3.49	0.35
PLSS	66.46	5.497	2.043	3.813	—	—	—	—	—	—
Pelvis	12.30	0.112	0.130	0.104	Hip	0/0	0/0	-45/-45	3.49	0.35
Upper leg	10.34	0.170	0.046	0.178	Knee	—	—	45/45	3.49	0.35
Lower leg	4.04	0.062	0.007	0.063	Ankle	0/0	0/0	0/0	3.49	0.35

^aSource: NASA.

The forces exerted by the astronaut on the capture bar in the normal direction are modulated by proportional-plus-derivative (PPD) control:

$$F_{Hn} = C_p(R - e) + C_d v \tag{4}$$

where *R* is the astronaut's maximum reach (0.67 m from shoulder to midpalm), *e* is the actual arm extension, *v* is the velocity of extension, and *C_p* and *C_d* are the proportional and derivative constants, set at 44 N/m and 50 Ns/m, respectively. The forces exerted by the astronaut in the tangential direction are calculated to provide a counter-rotary moment that balances the frictional forces on the capture bar. For the right-hand side, this force is

$$F_{HIR} = (1/2r_w)[(r_s - r_w)F_{tL} + (r_s + r_w)F_{tR}] \tag{5}$$

where *r_s* and *r_w* are the radii of the satellite interface ring and the capture bar manipulation wheel, respectively, and *F_{tL}* and *F_{tR}* are the left- and right-sided tangential forces, respectively.

It is assumed that the astronaut's feet are fixed in the inertial reference frame (i.e., clamped to the Space Shuttle foot restraint) and that his hands are attached to each side of the capture bar's manipulation wheel. Only the forces exerted by the astronaut's hands (rather than joint angles as in a forward kinematics approach) are prescribed because this mimics the actual task as described during EVA training.

To model human muscular actuation, all of the body joints are subject to passive PPD control during the inverse-kinematics phase. In the nominal range [Eq. (6)], the torque *τ_j* biases the joint angle *q_j* toward a predetermined value *q_b*. The subscript *j* is an index to indicate that there is a separate equation for each joint and each dof. When the joint exceeds the limits of its motion, *q_i*, it encounters joint stops modeled as stiff springs [Eq. (7)], with *k_i* set at 17.45 Nm/deg for all joint axes. The values for the nominal-range spring (*k_j*) and damping (*b_j*) constants are given in Table 1.

$$\tau_j = -k_j(q_j - q_b) - b_j \dot{q}_j \tag{6}$$

$$\tau_j = -k_i(q_i - q_j) \tag{7}$$

In the lower-body joints (sacroiliac to ankle), constants are higher to maintain posture, whereas the arm-joint constants are lower because the arms carry out most of the required motion. Because there are many redundant dof, body-joint angles are found using a linearized least-squares root solver.

Results

Figure 2 shows the motion of the capture bar. An initial negative yaw is quickly reversed as the left v-guide makes contact with the satellite at 0.8 s, followed by contact with the right v-guide at about 1.3 s. The *X* translation shows initial forward acceleration during the first 1.5 s, followed by some rebound and settling against the satellite interface ring and then a sustained push to the limit of the astronaut's reach envelope. The initial configuration of the astronaut's arms was 0.51 m of extension; therefore, the remaining 0.16 m of his reach

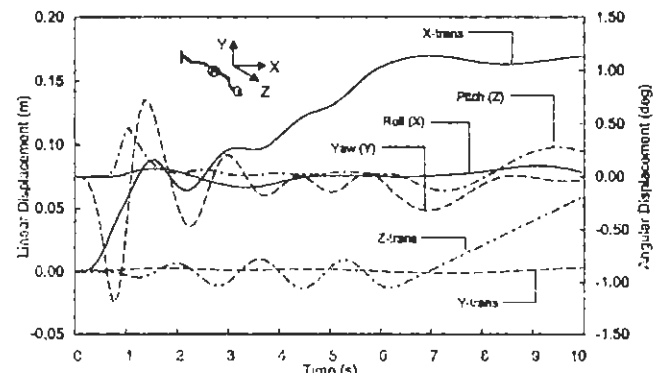


Fig. 2 Capture bar position vs time plot.

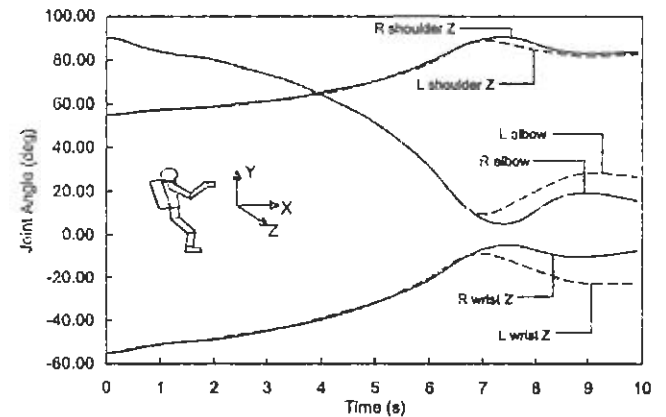


Fig. 3 Astronaut body joint position vs time plot.

envelope is quickly depleted. Contact between the capture bar and satellite begins at 0.7 s and lasts until 6.3 s.

Under pressure from the capture bar, the satellite accelerates away from the astronaut at 0.12 m/s² and acquires a final *X* velocity of 0.047 m/s. In addition, the satellite spin (roll) velocity is reduced from 6.02 to 5.55 deg/s, and yaw and pitch rates of -0.023 and 0.011 deg/s are imparted.

Figure 3 shows the astronaut's body-joint positions. The arms extend almost to the limit of the astronaut's reach, where contact is lost with the satellite, and the shoulder, elbow, and wrist *Z*-axis rotations stabilize around 80, 10, and -10 deg, respectively. (The remaining body-joint positions are not shown in Fig. 3 because they deviate less than 5 deg from the starting values.)

Joint torques calculated during the inverse-dynamics phase were found to be well within the astronaut's strength limits (100–200 Nm for most joint dof). In general, the greatest torques are experienced in the leg joints: -10.27 Nm in the left ankle and -10.28 Nm in both the left knee and left hip. The greatest torque experienced in the upper body was 8.98 Nm in the left shoulder.

Conclusion

The primary goal of this research effort was to demonstrate that a relatively complex EVA task could be simulated using computational multibody dynamics. The objective was not to showcase the full range of capabilities of computational simulation but rather to establish a testbed that could be used for further exploration of simulation techniques. Although the dynamic system itself is of a relatively high fidelity, some limitations remain. Most notable among these is the use of simple control laws to model astronaut hand forces and body torques. There exists an opportunity for additional work on simulations that employ more advanced control, including theory to account for the intelligence of the astronaut. Other limitations that should be addressed in future studies include a more scientific approach to the selection of control parameters and other constants, the influence of the EVA spacesuit on joint mobility, and compliance in the anchoring of the astronaut's feet (such as that expected from a portable foot restraint attached to the Orbiter's Remote Manipulator System).

In spite of these limitations, some important conclusions can be derived from this work. Figure 2 shows that the asymmetrical location of the capture bar's center of mass causes an initial yaw motion that brings the left-hand side of the capture bar into contact with the satellite before the right-hand side. As a result, roll and pitch disturbances are introduced that, together with the rebounds caused by the relatively noncompliant interface between the v-guides and the satellite interface ring, make it difficult for the astronaut to maintain the proper alignment between the capture bar and the satellite. In addition, the contact duration of 5–6 s was not sufficient to allow the satellite to rotate to the position where the capture bar latches would be triggered by structural elements on the satellite, an observation confirmed by video footage of STS-49. Furthermore, the slowing of the satellite's spin due to friction with the capture bar and the yaw and pitch rates caused by the unequal forces at the left and right contact points (also a consequence of the capture bar's center-of-mass asymmetry) could complicate further EVA capture attempts.

The fact that the satellite quickly translates out of reach when force is applied, combined with the observation of low torque values on body joints, indicates that a very light touch is required for this type of EVA task. Such a light touch may be difficult to apply because, according to EVA crewmembers, the spacesuit restricts tactility and proprioception, making it difficult to exert precision forces below a certain threshold (estimated to be as much as 40 N in the spacesuit).

A number of recommendations are suggested by the results of this simulation. For this type of task, astronauts should use very small, precise forces, even when dealing with objects of large mass. To compensate for the limited tactility allowed by a spacesuit, a mechanism such as the capture bar should be designed with additional compliance and minimal friction at the contact interface. Wherever possible, the center of mass of the manipulated object should be aligned with the center of the astronaut's task coordinates (i.e., the center of the manipulation wheel), even if this means adding mass. Finally, physical and computational simulators should be used in conjunction during EVA training so that each may help compensate for the limitations of the other.

Acknowledgments

This research effort is supported under NASA Grants NAGW-4336 and NAG5-4928. The authors wish to thank David Rahn and for his computer animation work; Robert Callaway and Bruce Webbon from NASA Ames Research Center and Mike Rouen, Joe Kosmo, Jim Maida, and Abilash Pandya from NASA Johnson Space Center for their encouragement and support; Mike Sherman and Dan Rosenthal of Symbolic Dynamics for technical assistance; and collaborators Norm Badler and Dimitris Metaxas.

References

- ¹Price, L. R., Fruhwirth, M. A., and Knutson, J. G., "Computer Aided Design and Graphics Techniques for EVA Analysis," *Proceedings of the Twenty-Fourth International Conference on Environmental Systems and Fifth European Symposium on Space Environmental Control Systems*, Society of Automotive Engineers, Warrendale, PA, 1994, pp. 1–13.
- ²"The McDonnell Douglas Human Modeling System MDHMS," Ver.

2.2, McDonnell Douglas Repts. MDC-93K0283 and MDC-93K0293, McDonnell Douglas Aerospace-West, Long Beach, CA, Sept. 1993, pp. 1–35.

³Pandya, A. K., Hasson, S. M., Aldridge, A. M., Maida, J. C., and Woolford, B. J., "Correlation and Prediction of Dynamic Human Isolated Joint Strength From Lean Body Mass," NASA TD-3207, June 1992.

⁴Newman, D. J., and Schaffner, G., "Computational Dynamic Analysis of Extravehicular Activity: Large-Mass Handling," *Journal of Spacecraft and Rockets*, Vol. 35, No. 2, 1998, pp. 225–227.